Research Article | Vol. 12, No. 6 / 1 June 2021 / Biomedical Optics Express 3684
Biomedical Optics EXPRESS

Large-scale, cell-resolution volumetric mapping allows layer-specific investigation of human brain cytoarchitecture

IRENE COSTANTINI,[1,2,3,9,*] GIACOMO MAZZAMUTO,[1,3,9] MATTEO ROFFILLI,[4] ANNUNZIATINA LAURINO,[1,8] FILIPPO MARIA CASTELLI,[1,5] MATTIA NERI,[4] GIOVANNI LUGHI,[4] ANDREA SIMONETTO,[4] ERICA LAZZERI,[1] LUCA PESCE,[1,5] CHRISTOPHE DESTRIEUX,[6] LUDOVICO SILVESTRI,[1,3,5] VALERIO CONTI,[7] RENZO GUERRINI,[7] AND FRANCESCO SAVERIO PAVONE[1,3,5]

[1] *European Laboratory for Non-Linear Spectroscopy (LENS), University of Florence, Sesto Fiorentino, Italy*
[2] *Department of Biology, University of Florence, Italy*
[3] *National Institute of Optics (INO), National Research Council (CNR), Sesto Fiorentino, Italy*
[4] *Bioretics srl, Cesena, Italy*
[5] *Department of Physics, University of Florence, Italy*
[6] *UMR 1253, iBrain, Université de Tours, Inserm, Tours, France*
[7] *Pediatric Neurology, Neurogenetics and Neurobiology Unit and Laboratories, A. Meyer Children's Hospital, University of Florence, Florence, Italy*
[8] *Present address: Department of Neurofarba, Section of Pharmacology and Toxicology, University of Florence, Italy*
[9] *These authors contributed equally to this work*
[*] *costantini@lens.unifi.it*

Abstract: Although neuronal density analysis on human brain slices is available from stereological studies, data on the spatial distribution of neurons in 3D are still missing. Since the neuronal organization is very inhomogeneous in the cerebral cortex, it is critical to map all neurons in a given volume rather than relying on sparse sampling methods. To achieve this goal, we implement a new tissue transformation protocol to clear and label human brain tissues and we exploit the high-resolution optical sectioning of two-photon fluorescence microscopy to perform 3D mesoscopic reconstruction. We perform neuronal mapping of 100mm^3 human brain samples and evaluate the volume and density distribution of neurons from various areas of the cortex originating from different subjects (young, adult, and elderly, both healthy and pathological). The quantitative evaluation of the density in combination with the mean volume of the thousands of neurons identified within the specimens, allow us to determine the layer-specific organization of the cerebral architecture.

1. Introduction

The three-dimensional reconstruction of large volumes of human brain tissue at cellular resolution remains one of the biggest technical challenges of neuroscience. Nowadays, structural analyses are obtained using traditional processes based on 2D evaluation of thin slices, but they still suffer from significant drawbacks. Such limitations are inherent to the bidimensional nature of the classical slide-based preparations and include: low sensitivity for sparse features, difficult assessment of dimensions, alteration of morphology, visual artifacts (different orientation or distribution), and sampling bias. To overcome the image depth limit and obtain high-resolution reconstructions of whole mouse brain samples, several optical imaging combined with histological techniques have been developed. Micro-optical sectioning tomography (MOST) [1–4], serial

#415555 https://doi.org/10.1364/BOE.415555
Journal © 2021 Received 1 Mar 2021; revised 23 Mar 2021; accepted 30 Mar 2021; published 27 May 2021

Biomedical Optics EXPRESS

two-photon tomography (STP) [5], and block-face serial microscopy (FAST) [6], which exploit a combined system of slicing and imaging, are examples of these approaches. In particular, the Mouselight platform based on STP [7], and FAST use a vibratome for the slicing process, allowing whole-brain imaging at a subcellular resolution. Despite the substantial advantages prompted by automatic histology instrumentation and serial sectioning [8], lack of three-dimensionality affects the quality of the produced data and reliability of the analysis.

Recent advances in tissue imaging — in terms of optical clearing, fluorescent staining, and microscopy techniques — have paved the way to high-resolution 3D reconstruction of the brain [9]. The combination of clearing methodologies and cutting-edge microscopies techniques as light sheet microscopy enables the reconstruction of large volumes of tissue and even entire organs [10–12]. Indeed, tissue clearing makes antigens and light penetrate deep inside the sample, enabling fluorescence imaging through high-resolution optical techniques. Multiple methods have been developed to achieve sound clearing and homogeneous staining, but only a few of them have been applied to human tissue. Such samples, in particular archived materials, present specific challenges in comparison to animal models: variability of post-mortem fixation conditions, presence of blood inside the vessels, autofluorescence signals coming from lipofuscin-type pigments, and, finally, the need of exogenous labeling [13]. Alteration of antigens, due to fixation and/or long storage, prevent good immunostaining recognition. Normally, diffusion limits the homogeneous penetration of the dye inside the tissue; voluminous macromolecules, like antibodies, can penetrate only a few dozens of microns inside the sample. Among the various techniques that favor diffusion and increase tissue transparency, tissue transformation techniques such as the CLARITY method [14] and its adaptations have had considerable success. However, they also have limitations. Some were developed for application only to specific samples: e.g. pediatric tissue or controlled post mortem fixation conditions [15,16]. Others demonstrated compatibility with few antibodies and/or can achieve a staining depth of only a few tens of microns and/or are characterized by very long clearing time [17–22]. Indeed, prolonged formalin-fixed materials are really difficult to clear with only SDS treatment. Different authors [18,21] point out the necessity of performing a prolongation of the delipidation step up to several months in these cases. Recently, ELAST was introduced [23], a technology that transforms tissues into elastic hydrogel allowing the homogeneous staining of 1 cm-thick sections with various antibodies; however, the preparation of the sample requires sophisticated custom-made equipment and long processing time (20 days). Organic-based techniques were adapted to clear and label human brain tissue, but also in this case they need specific sample preparations: fresh-frozen samples [24], fetal brains [25], or in-situ controlled perfusion fixation [26,27]. In conclusion, up to now, we have no flexible strategy for fast clearing of human brain specimens from different ages, formalin-fixed for a long time, and compatible with different antibodies labelling. An additional consideration that needs to be addressed is that the advances in tissue clearing need large-scale data analysis and management. Indeed, high-throughput computational approaches are required to scale-up the processing of the significant amount of data produced by 3D anatomical reconstructions obtained by the combination of clearing techniques with high-resolution optical methods.

Considering the difficulties of human tissue labeling that decrease the quality of the produced images, cell recognition in thick samples is very arduous with conventional microscopy. Here we propose a new clearing method that in combination with an advanced optical microscopy technique enables the reconstruction of mesoscopic volumes of the human brain at sub-micron resolution and the study of the anatomical organization of neurons in 3D. First, we implement a novel flexible methodology, the SWITCH/TDE protocol, to perform reliable clearing and labeling of human cortical tissues. Following this clearing protocol, we exploit the high-resolution optical sectioning of Two-Photon Fluorescence Microscopy to perform 3D mesoscopic imaging of human brain samples. To analyze the large amount of generated data, we apply different software tools to process the images in an automated fashion and extract reliable and quantitative information.

Biomedical Optics EXPRESS

A custom-made software called ZetaStitcher is used to stitch together the 3D tiles acquired with the TPFM microscope. Then a 2.5D Machine Learning method based on a Convolutional Neural Network is used to automatically segment the neurons in 3D to extract quantitative data (both cell counting and cell volume reconstruction). The volumetric assessment, together with cell counting, obtained with this approach allows us to extract morphological information such as cell density, cell localization, cell average volume, and cell volumetric density, and discriminate the layer organization of the cerebral cortex. We demonstrate the applicability of the approach by reconstructing and analysing four different areas of the human cortex originating from different subjects (young, adult, and elderly, both healthy and pathological).

2. Methods

2.1. Human brain specimen collection

The study was approved by the Pediatric Ethic Committees of the Tuscany Region (under the project RF-2013-02355240 funded by the Italian Ministry of Health and the Tuscany Region). Healthy tissue samples were obtained from the body donation program (Association des dons du corps) of Université de Tours and from the Body Donation Program "Donation to Science" of the University of Padova. Prior to death, participants gave their written consent for using their entire body – including the brain – for any educational or research purpose in which anatomy laboratory is involved. The authorization documents (under the form of handwritten testaments) are kept in the files of the Body Donation Program. Pediatric human brain samples were removed during surgical procedures for the treatment of drug-resistant epilepsy in children with malformations of cortical development (MCD). Samples were obtained after informed consent, according to the guidelines of the Pediatric Research Ethics Committee of the Tuscany Region. Upon collection, samples were placed in neutral buffered formalin (pH 7.2–7.4) (Diapath, Martinengo, Italy) and stored at room temperature until the transformation and clearing process. The four specimens analyzed in the study were formalin fixated respectively for 6-months, 1-year, 4-years and 5-years. The specimen shown in Fig. 1 was fixated for 7-years (the staining procedures with the antibodies of Fig. 1 were performed on cut pieces of this sample).

2.2. SWITCH/TDE clearing and labelling protocol

Blocks of fixed samples were washed with a Phosphate Buffered Saline (PBS) solution at 4°C with gentle shaking for one month to remove formalin from the tissue. Blocks were embedded in a low melting agarose (4 % in 0.01M PBS) and cut into (450 ± 50) μm coronal sections with a vibratome (Vibratome 1000 Plus, Intracel LTD, UK). After the cutting, the agarose surrounding each slice was removed. The permeabilization and staining protocols were modified from that of Murray et al. 2015 [19], as described below. Samples were first incubated in the ice-cold SWITCH-OFF solution (4 % GA in PBS 1X and KHP 0.1M, titrated with HCl to pH = 3) for 1 day at 4°C with gentle shaking, then incubated for 1 day in the SWITCH-ON solution (0.5 % GA in PBS 1X, pH = 7.6) for 1 day at 4°C with gentle shaking. After two washing steps in the PBST solution (PBS with 1 % Triton X-100, pH = 7.6) for 4 hours at room temperature (RT), the samples were inactivated with a solution of 4 % w/v acetamide and 4 % w/v glycine with a pH = 9 (overnight incubation at 37°C). Two washing steps in PBST solution for 4 hours at room temperature (RT) were performed before the incubation in the Clearing Solution (200mM SDS, 20mM Na_2SO_3, 20mM H_3BO_3, pH = 9) at 70°C for lipids removal. Incubation time in clearing solution was adapted depending on tissue characteristics: samples from pediatric patients were kept overnight (6-8 hours), while samples from adult and elderly subjects up to one day, until complete transparency was achieved. Two washing steps in the PBST solution for 8 hours at room temperature (RT) were performed to prepare the sample for the labeling process. Primary antibodies were incubated in the PBST solution for one day at 4°C. After two washing steps

Biomedical Optics EXPRESS

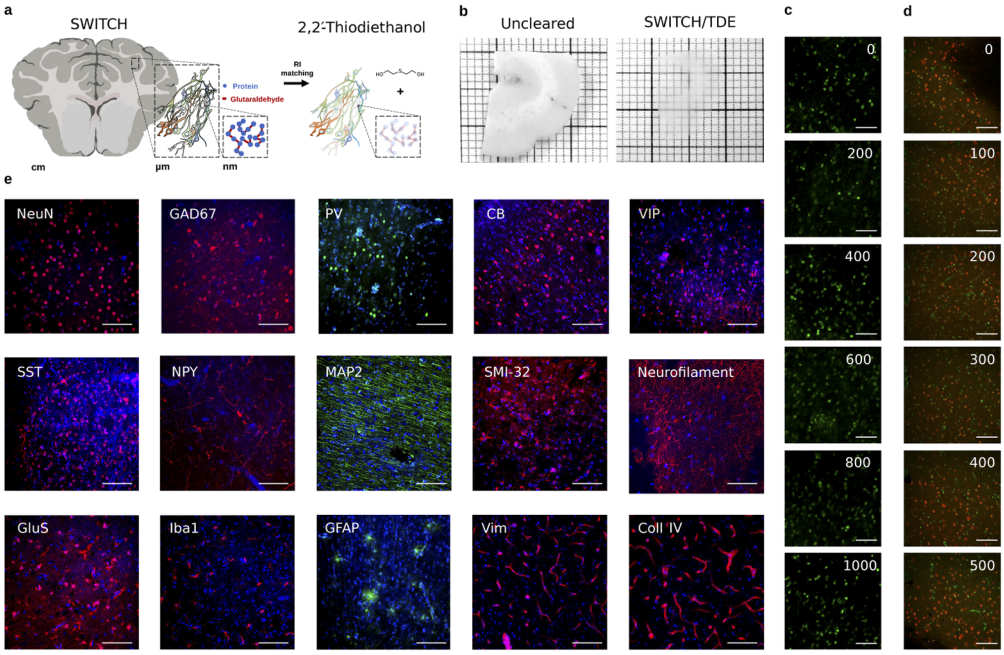

Fig. 1. (a) Schematic illustration of the SWITCH/TDE clearing method. (b) 1 mm-thick slice of an adult human brain sample before and after the treatment. (c) Images of SYTOX Green labeled tissue at different depths. Scale bar = 100 µm. (d) Images of NeuN immunostained tissue at different depths. Scale bar = 50 µm. Acquisition obtained with TPFM. (e) Representative images of cleared tissues immunostained with various antibodies and DAPI (4′, 6-Diamidino-2-Phenylindole, Dihydrochloride). Scale bar = 50 µm. Acronym list: Neuron-specific Nuclear protein (NeuN, all neurons), Microtubule-Associated Protein 2 (MAP2; pyramidal cells), Nonphosphorylated neurofilament protein (SMI32; pyramidal cells), Glutamic Acid Decarboxylase (GAD67; all GABAergic interneurons), Parvalbumin (PV; GABAergic interneurons subtype), Calbindin (CB; GABAergic interneurons subtype), Vasointestinal peptide (VIP; GABAergic interneurons subtype), Somatostatin (SST; GABAergic interneuron subtype), Neuropeptide Y (NPY; GABAergic interneuron subtype), Neurofilament (NF), Ionized calcium Binding Adaptor molecule 1 (Iba1; glial cells), Glial Fibrillary Acidic Protein (GFAP; glial cells), Glutamine synthetase (GluS), Vimentin (Vim; Microvasculature), Collagen IV (Coll IV; microvasculature).

Biomedical Optics EXPRESS

in the PBST solution for 8 hours at RT, secondary antibodies were incubated in PBST for one day at RT. Table 1 reports the list of antibodies and dilutions used. After two washing steps of 8 hours with PBST at RT, samples were fixed with a 4 % solution of paraformaldehyde (PFA) for 10min at 4°C to avoid antibody detachment. Samples were then washed three times with PBS for 10min at RT to remove the excess of PFA. Optical clearing consists in incubation in solutions of increasing concentrations of 20 %, 40 % and 68 % (vol/vol) of 2, 2′-thiodiethanol in 0.01M PBS (TDE/PBS), each for 1 day at room temperature (RT) with gentle shaking. For nuclear staining, DAPI or SYTOX Green were diluted in the last incubation of the sample in the 68 % (vol/vol) TDE/PBS solution. For 1 mm thick samples, the incubation was performed for two days. Finally, samples were mounted in a custom made chamber with UV silica cover slip (UQG Optics, CFS-5215) that flattens the sample while keeping it completely covered by the TDE/PBS solution allowing a perfect RI matching which is essential for imaging. Sample pictures before and after the clearing process were acquired using a digital camera (Sony DSC-WX500), samples were kept soaked either in PBS or TDE.

Table 1. Table summarizing the dyes tested in this study. The P/M column denotes polyclonal vs monoclonal antibodies. The same abbreviations used in Fig. 1 are used. AF is a shorthand for Alexa Fluor.

Molecule	Company	Cat. n.	Host	P/M	Dilution
NeuN	Merck	ABN91	Chicken	P	1:50
GAD67	Santa Cruz	sc-28376	Mouse	M	1:200
GAD65/67	St John's Lab	STJ93195	Rabbit	P	1:200
PV	Abcam	ab11427	Rabbit	P	1:200
PV	Abcam	ab32895	Goat	P	1:200
CB	Abcam	ab207528	Rabbit	M	1:200
VIP	Abcam	ab214244	Rabbit	M	1:200
SST	Abcam	ab30788	Rat	M	1:200
NPY	Abcam	ab6173	Sheep	P	1:200
NPY	Abcam	ab112473	Mouse	M	1:200
SMI-32	Merck	NE1023	Mouse	M	1:200
Neurofilament	Abcam	ab4680	Chicken	P	1:200
GluS	Merck	MAB302	Mouse	M	1:200
MAP2	Abcam	ab5392	Chicken	P	1:200
GFAP	Abcam	ab194324	Rabbit	M	1:200
Iba1	Abcam	ab195031	Rabbit	M	1:200
Coll IV	Abcam	ab6586	Rabbit	P	1:200
Vim	Abcam	ab8069	Mouse	M	1:200
Anti-Rat IgG, AF 568	Abcam	ab175475	Donkey	P	1:200
Anti-Rabbit IgG, AF 568	Abcam	ab175470	Donkey	P	1:200
Anti-Chicken IgY, AF 568	Abcam	ab175711	Goat	P	1:200
Anti-Mouse IgG, AF 568	Abcam	ab175700	Donkey	P	1:200
Anti-Sheep IgG, AF 568	Abcam	ab175712	Donkey	P	1:200
Anti-Rabbit IgG, AF 488	Abcam	ab150077	Goat	P	1:200
Anti-Chicken IgY, AF 488	Abcam	ab150169	Goat	P	1:200
DAPI	Thermo Fisher Scientific	D1306			1:1000
SYTOX Green	Thermo Fisher Scientific	S7020			1:1000

Biomedical Optics EXPRESS

2.3. Two-photon fluorescence microscopy

A custom-made Two-Photon Fluorescence Microscope (TPFM) was built in order to enable mesoscopic reconstruction of cleared samples. A mode-locked Ti:Sapphire laser (Chameleon, 120 fs pulse width, 80 MHz repetition rate, Coherent, CA) operating at 800 nm was coupled into a custom-made scanning system based on a pair of galvanometric mirrors (LSKGG4/M, Thorlabs, USA). The laser was focused onto the specimen by a refractive index tunable 25× objective lens (LD LCI Plan-Apochromat 25×/0.8 Imm Corr DIC M27, Zeiss, Germany). The system was equipped with a closed-loop XY stage (U-780 PILine XY Stage System, 135 × 85 mm travel range, Physik Instrumente, Germany) for radial displacement of the sample and with a closed-loop piezoelectric stage (ND72Z2LAQ PIFOC objective scanning system, 2 mm travel range, Physik Instrumente, Germany) for the displacement of the objective along the z-axis. The fluorescence signal was collected by two independent GaAsP photomultiplier modules (H7422, Hamamatsu Photonics, NJ). Emission filters of (440 ± 40) nm, (530 ± 55) nm and (618 ± 25) nm were used to detect the signal, respectively, for DAPI, Sytox Green/Alexa 488, and Alexa Fluor 568. The instrument was controlled by a custom software, written in LabView (National Instruments, TX) able to acquire a whole sample by performing z-stack imaging (depth = (500 ± 100) μm) of adjacent regions with an overlap of 40 μm and a voxel size of $0.88 \times 0.88 \times 2$ μm. The acquisition was performed using a FOV of 450 μm resulting in 512*x*512 px images that were saved as TIFF files. The microscope is characterized by a dwell time of 5 μs resulting in 1.31s per image, and 5.46 minutes per stack of 500 μm depth. Therefore the acquisition of the four samples took from 11 hours to 30 hours of continuous imaging.

2.4. Volumetric image stitching

To obtain a single file view of the sample imaged with the TPFM, the acquired stacks were fused together using the ZetaStitcher tool [28]. This software can take advantage of the overlap between neighboring stacks to correct the mechanical error of the imaging platform. Indeed, mesoscopic reconstruction with TPFM can take several days, and temperature changes and mounting medium evaporation can lead to some micron-scale distortion. The software is based on two steps: an alignment process followed by image fusion. As a first step, a 2D cross-correlation map is evaluated at several depths for every pair of adjacent 3D stacks, moving each stack relative to its neighbor. The final position of all stacks is determined by applying a global optimization algorithm to the displacements of the individual pairs. Finally, the stacks are fused into a 3D reconstruction of the whole sample stored in a single TIFF file. The raw datasets of the four samples under investigation in this paper are made available on the EBRAINS platform provided by the Human Brain Project [29].

2.5. Automatic cell counting and segmentation

We used a 2D Convolutional Neural Network for pixel-based classification expanding on the design employed in a previous work [30]. In this network architecture, $32 \times 32 \times 2$ sized patches (i.e. considering red and green channels) are extracted from the stitched volume, and fed to the CNN model after a preprocessing step consisting of a single 5×5 gaussian kernel filtering stage with $\sigma = 3$. This operation replicates the intrinsic blurring caused by resampling during data augmentation in the training phase of the CNN. The neural network architecture consists of three convolutional layers, the first two of which are followed by 2×2 max-pooling downsampling, and three fully connected layers, the last of which makes use of a two-class softmax activation function. A block diagram of the overall network structure as well as the trainable parameters (205 024 in total) and optimizer hyper-parameters are described in the supplementary information. The so-defined CNN model classifies the central pixel of each input patch by exploiting the visual pattern of the local neighbourhood (i.e. the coloured 32×32 texture) to which the pixel belongs. The model can be used for efficient inference on input data larger than the 32×32 patches by

Biomedical Optics EXPRESS

exploiting formal equivalence, named fully convolutional, between fully connected layers and 1×1 convolutions [31]. This allows us to efficiently produce heatmaps (i.e. probability maps) of entire stack frames. These two-dimensional maps are reassembled back into a 3D stack to obtain an estimate of the three-dimensional probability distribution of neuronal soma presence. In particular, the obtained heatmaps are processed with two different filtering modalities in order to optimize either cell counting or volumetric evaluation.

For cell counting, a 2D morphological erosion with 3×3 kernel is applied independently to each 2D heatmap before the 3D reconstruction in order to optimize the separation of touching neurons. For volume evaluation, the heatmap stack undergoes a post-processing step of false positive reduction with the application of a 5×5 median filter and a gray-scale morphological opening with a 3×3 structuring element. We consider the isosurfaces of this field corresponding to a 0.55 statistical threshold to be representative of the physical boundaries of neuron soma; to calculate them we use a custom variant of the Marching Cubes algorithm [32] followed by additional topological fixes on the identified objects to ensure that every soma is represented by a 2-manifold watertight mesh. This approach allows us to retrieve a three-dimensional vectorial reconstruction of the segmented objects in the entire z-stack, although limited by a grouping effect

Table 2. Number, mean volume and density of the neurons in the six layers and in the total volume of the cortex for each four specimen.

	Layer	N. Neurons	Tissue volume (mm^{-3})	Density (10^3 mm^{-3})	Mean Volume (μm^3)	Filling fraction
Specimen 1						
	1	47329	2.880	17	2603	1.38 %
	2	11580	0.486	33	2916	3.87 %
	3	40684	1.758	27	4441	5.02 %
	4	47433	1.814	31	3549	4.90 %
	5	23290	1.300	24	4358	4.68 %
	6	13843	0.769	22	2263	1.99 %
	tot.	184159	9.007	24	3569	21.8 %
Specimen 2						
	1	178432	11.533	16	2550	1.5 %
	2	193783	11.724	17	2567	1.8 %
	3	219289	12.789	18	2922	2.3 %
	4	97771	2.413	51	2730	6.5 %
	5	78402	2.199	43	3324	6.4 %
	6	41167	1.054	47	1989	3.8 %
	tot.	808844	41.712	20	2740	22.4 %
Specimen 3						
	1	34997	1.646	21	2105	1.8 %
	2	36697	1.432	26	3412	5.3 %
	3	66012	3.464	19	4627	5.7 %
	4	46979	1.804	26	3524	5.8 %
	5	55617	2.387	23	4584	6.4 %
	6	16912	5.656	3	3410	1.9 %
	tot.	257214	16.389	16	3853	26.9 %
Specimen 4	tot.	177286	12.694	14	3008	4.2 %

Biomedical Optics EXPRESS

that sometimes emerges after the instance segmentation step: neurons that are too close to each other are sometimes identified as a single unit. All the 2.5D computations have been performed on a standard Linux-based workstation equipped with the ALIQUIS software ecosystem [33], using Google TensorFlow as the CNN backend [34].

The ground truth was annotated by two distinct operators on LAIRA, a web-based collaborative application [35]. By following an Active Learning paradigm [36] the network was incrementally trained against a number of positive and negative samples originating from the four specimens to improve inter-specimen statistical representatives: the final training dataset is composed of 112 images of 512×512 px, corresponding to 450×450 μm, for a total of 7312 manually annotated neurons (1180 from the first annotation without Active Learning). 14 independent images (1505 neurons) were used to validate the CNN and an additional 14 images (1208 neurons) to test it. Model regularization is provided in the form of dropout layers, each with a dropout factor of 0.5. The manually annotated ground truth used to train the neural network is also made available for download on the EBRAINS platform [29] in Ximage format [37] (see Supplement 1 and Dataset 1 [38]).

2.6. Data analysis

The physical boundaries of the neuronal soma were stored in the form of triangular meshes in Alembic [39] binary file format, which is suitable for rendering and for further analysis. These files were then processed with Python scripts.

For volumetric evaluation, thresholds were applied to remove segmentation artifacts: volumes lower than 400 μm^3 and higher than 12000 μm^3 were discarded. To visualize neuronal count, density and mean volume distributions of the analyzed samples, we plotted histograms using 3D moving bins of $100 \times 100 \times 100$ μm as shown in Fig. 4. The centroid of the identified meshes was used to assign each object to their corresponding histogram bin. Then, using the masks that were manually drawn for each cortical layer (Fig. S11 in Supplement 1), we extracted cell counts and densities as shown in Table 2.

3. Results

3.1. SWITCH/TDE clearing and labeling approach

Penetration of macromolecules and light deep inside the sample are critical processes that are necessary to obtain homogeneous staining of the sample and to reach high transparency, which is essential to perform 3D optical reconstruction with fluorescence imaging. In order to obtain a reliable methodology to label and clear human brain samples from different regions, subjects, and fixation conditions, we modified the SWITCH tissue transformation protocol [19] and we combined it with the 2, 2′-thiodiethanol (TDE) clearing method [15] (Fig. 1(a)). Amongst the various techniques, we decided to use the SWITCH methodology since it allows to control the chemical interaction time and kinetics taking place inside the tissue. By modifying the solutions used during the fixation and clearing, we achieved more uniform processing of tissues up to 1 mm. At first, we optimized the fixation condition during the SWITCH protocol lowering the concentration of glutaraldehyde (from 1 % to 0.5 %) during the SWITCH ON step (data not shown). Then, depending on tissue characteristics, we incubated the different samples in the SWITCH clearing solution at 70°C from 6 hours to one day. Finally, we used the aqueous agent TDE to reduce the Refractive Index (RI) inhomogeneity between the tissue and the surrounding medium, thus minimizing the scattering of light and guaranteeing the final transparency of the sample (Fig. 1(b)). Differently from our previous paper [15], we used one-day serial incubations at Room Temperature (RT) up to a concentration of 68 % TDE in Phosphate Buffered Saline (PBS) to obtain homogeneous clearing of both grey and white matter. The final solution is characterized by a refractive index of 1.46 equal to that of the UV silica glass used for imaging.

Biomedical Optics EXPRESS

The combination of the two techniques allows deep tissue imaging with Two-Photon Fluorescence Microscopy (TPFM): small molecules as SYTOX Green can be imaged up to 1 mm in-depth, while antibodies can homogeneously label 500 μm-thick slices, respectively (Figs. 1(c), d). Finally, we demonstrated the compatibility of the SWITCH/TDE method with human brain immunostaining using a variety of different antibodies (Table 1), which were able to stain neuronal cells, GABAergic interneurons and interneurons subtypes, neuronal fibers, glial cells, and microvasculature. Incubation time and temperature parameters optimizations are described in the supplementary materials (Fig. S1 in Supplement 1). Representative images of the different staining are shown in Fig. 1(e).

3.2. 3D reconstruction of cerebral cortex samples

The SWITCH/TDE protocol is able to clear different areas of the human brain cortex from subjects of different ages (pediatric, adult, and elderly), obtained from biopsies collected during epilepsy surgery interventions or autopsy stored up to 7 years in formalin (Fig. S1 in Supplement 1). To demonstrate the versatility of the method, four different human brain specimens, from healthy and diseased patients, were analyzed. Two different portions of the left prefrontal cortex from an adult (Male, 67 years old, sample 1) and an elderly subject (Female, 99 years old, no Alzheimer's disease but initial cognitive decline, no hypertension; sample 2); one dysplastic brain sample from the left temporo-occipital cortex of a 29-year-old man operated to treat drug resistant epilepsy due to focal cortical dysplasia Type IIa (FCDIIa), and one dysplastic brain sample from the left temporo-parietal cortex of an eight-year-old boy operated to treat drug resistant epilepsy due to hemimegalencephaly (HME), respectively samples 3 and 4. The samples were treated with the SWITCH/TDE clearing method and immunolabeled with the Neuron-specific Nuclear protein (NeuN) to detect neurons and DAPI for nuclear staining (sample area of $\approx 1 \times 1$ cm^2 and depth of ≈ 500 μm). Imaging was performed with a custom-made Two-Photon Fluorescence Microscope designed to perform mesoscopic reconstruction with a resolution of $(0.88 \times 0.88 \times 2)$ μm, see Fig. 2 and Fig. S3 in Supplement 1. After the acquisition, adjacent stacks were aligned and merged together by evaluating the cross-correlation of the overlapping areas using a custom-made stitching software called ZetaStitcher [28].

3.3. Neuronal distribution analysis

The volumetric 3D reconstruction obtained with the TPFM consists of tens of GB of data. In particular, the fused volumes of the four samples acquired in this work are sized 19, 50, 57 and 52 GB. Moreover, the image contrast variability in the different samples prevented the use of traditional methods (Fig. S4 in Supplement 1). Therefore, to automatically obtain quantitative information from the 3D reconstruction of the samples imaged with the TPFM, we used a 2D Convolutional Neural Network for pixel-based classification expanding on the design employed in a previous work [30].

The so-called 2.5D approach allowed us to perform both cell counting and cell volumetric segmentation using different parameters. A detailed description of the method can be found in the method section and in the supplementary material (Figs. S5, S6, in Supplement 1 and Visualization 1). The statistical assessment of the 2.5D performance was determined by analyzing four representative stacks of $100 \times 100 \times 100$ μm, one for each specimen, and a representative stack of $100 \times 100 \times 450$ μm to determine the accuracy along with the full depth (Fig. S7 in Supplement 1). The total number of neurons found by the 2.5D method is 442 over the 474 neurons annotated in the GT, and the volumetric evaluation of the neurons is characterized by a precision and a recall rate respectively, equal to (91 ± 7) % and (96 ± 3) %. To verify the stability of the 2.5D approach along the tissue depth, we plotted the z-profiles for cell counts, mean volume, and volumetric density across different regions of the cortex along 10 different

Biomedical Optics EXPRESS

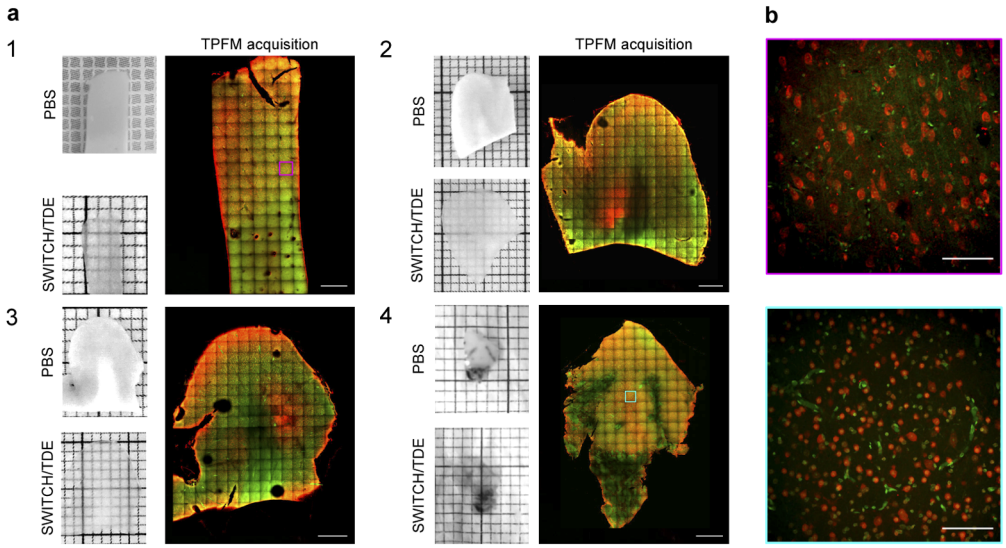

Fig. 2. (a) Pictures showing the four analyzed human brain specimens before and after SWITCH/TDE clearing. A representative middle plane ($z \approx 200$ μm) of the mesoscopic reconstruction obtained with TPFM is shown next to each specimen. Scale bar = 1 mm. Specimens 1 and 2: two different portions of the left prefrontal cortex from adult and elderly subjects. Specimens 3 and 4: two surgically removed pieces from patients affected by Focal Cortical Dysplasia Type 2a (FCDIIa) and by Hemimegalencephaly (HME), respectively. (b) Magnified insets of specimen 1 (magenta) and 4 (cyan) showing the native resolution of the acquisition. Tissues were stained with an anti-NeuN antibody (in red) and with DAPI (in green). Scale bar = 100 μm

lines that were manually drawn orthogonally to the cortical layers in specimens 1, 2, and 3 (Figs. S8-S11 in Supplement 1).

The four datasets acquired with the TPFM were processed with the 2.5D automatic segmentation method, obtaining meshes for every single neuron in the whole volume (Visualization 2). Figure 3 shows a 3D rendering of the meshes for each processed specimen. The rendering highlights the anatomical architecture of the six cortical layers. To characterize the structural organization in the analyzed tissues, we calculated the cell density, the mean volume, and the volumetric density distributions. The corresponding maps were obtained, for each specimen, with a 3D moving average of $100 \times 100 \times 100$ μm with a binning of 10 μm (Fig. 4(a), b, c). The images show the presence of different peaks along with the cortical depth. In particular, volume profiles show peaks in layers 3 and 5, while the neuronal density has peaks in layers 2 and 4. Figures S8-S11 in Supplement 1 show 10 representative profiles for each specimen characterizing the trend of the distributions in different areas of the cortex. Finally, we calculated the densities and the percentage of neuronal counting and mean volume for the total volume of the grey matter of the sample. To do that, a mask for the grey matter of each sample was manually drawn. To quantify the neuronal distribution along with the six cortical layers, masks of each layer volume were manually drawn for each sample (Fig. S12 in Supplement 1). The HME biopsy (sample 4) showed a disruption of the structural organization of the cortex, making layer classification impossible. The results of counting and mean neuronal volumetric assessment are shown in Table 2, numbers are provided for the overall volume and divided into the six cortical layers.

Biomedical Optics EXPRESS

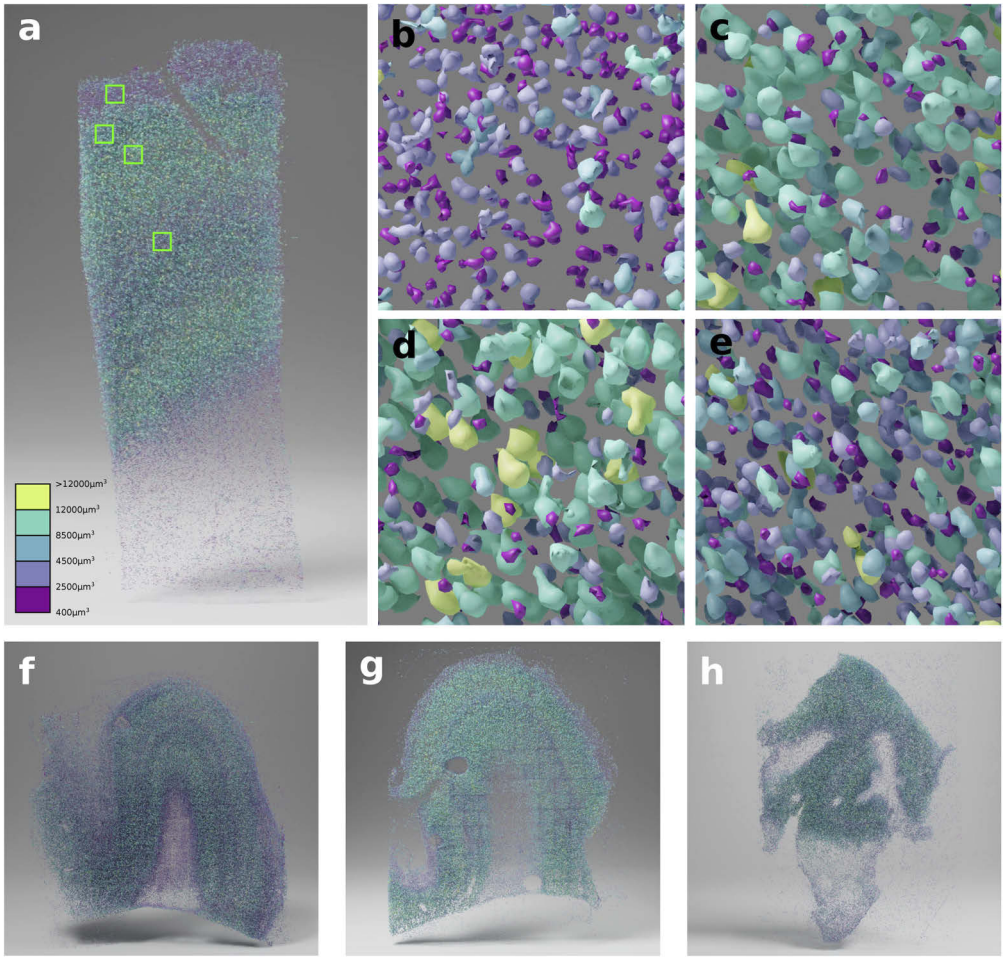

Fig. 3. Panels a, f, g, h show the 3D rendering for specimens 1, 2, 3 and 4 respectively. The magnified view of the highlighted squares in panel a from top to bottom are shown in panels b, c, d, e, highlighting the neuronal size and density in the different cortical layers.

Biomedical Optics EXPRESS

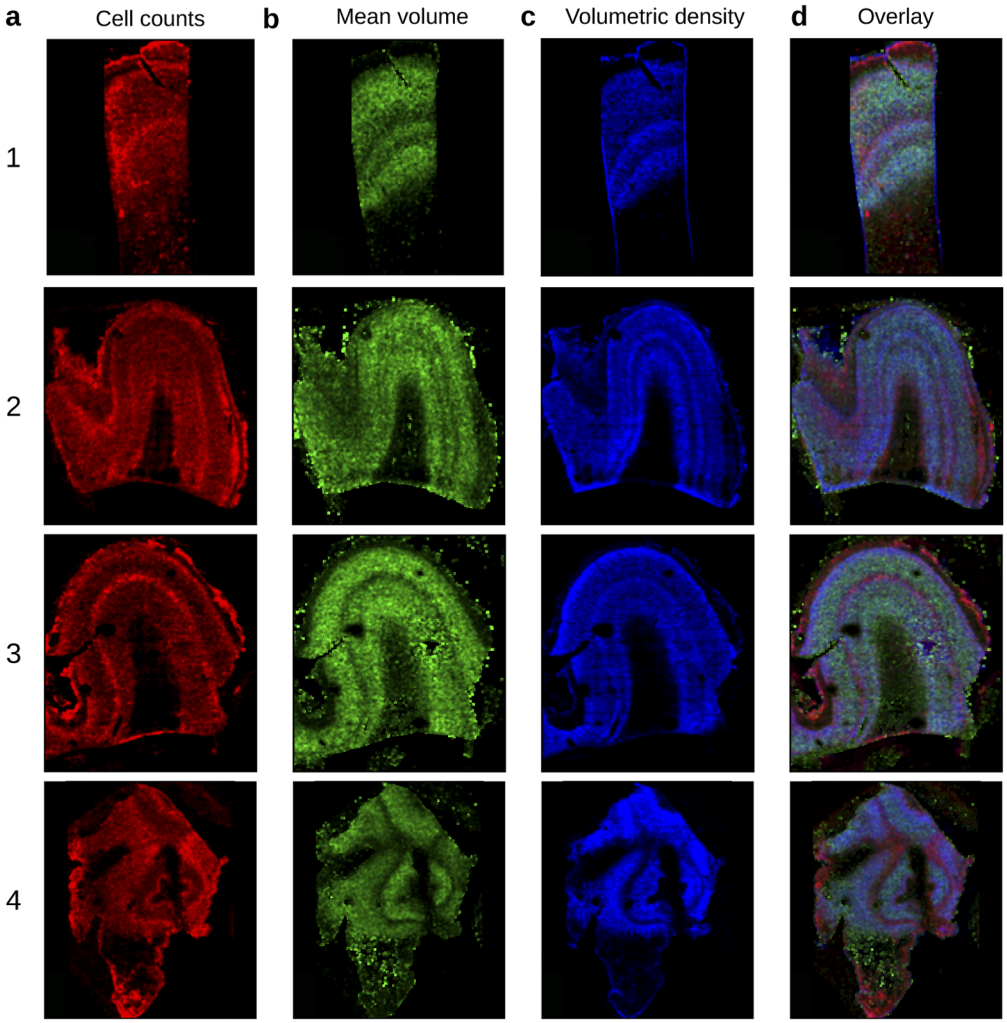

Fig. 4. Representative distribution maps of the cell counting (a), mean volume (b), volumetric density (c), and overlay of the three maps (d) of the middle plane of each specimen.

Biomedical Optics EXPRESS

4. Discussion and conclusion

In this work, addressing some of the most critical challenges of human brain mapping (i.e., sample preparation, mesoscopic reconstruction at high resolution, and big data analysis), we enabled a 3D characterization of the cytoarchitecture of the tissue at high resolution. In comparison to animal brains, human neural tissues present high variability of post-mortem fixation conditions and antigens alterations that prevent proper immunostaining recognition. In this work, we combined the SWITCH tissue transformation method with the TDE clearing. The SWITCH technique removes lipids from the sample while maintaining structural integrity, leading to an increase of tissue permeability and a reduction of the tissue refractive index (RI). The TDE clearing method homogenizes the RI of the sample with that of the mounting medium to reach the final transparency. The optimized protocol can perform a rapid and efficient tissue clearing and homogeneously stain the tissue with small molecules (up to 1 mm in-depth) as well as antibodies (up to 500 μm). We provided a table of tested antibodies and molecules suitable with the protocol for neuronal and non-neuronal cells as well as blood vessel staining. The compatibility with different staining demonstrates the preservation of the tissue's structure. Indeed, the protocol, unlike others, does not employ aggressive denaturant agents which can affect the tissue architecture and antigenicity of endogenous biomolecules. [9]. In addition, the SWITCH treatment, using the GA to protect the tissue integrity and a high temperature to remove the lipids, allows to speed up the delipidation process and complete it in 4-5 days (considering also the fixation in GA), overcoming the limitation of using direct SDS treatment, that in prolongated formalin-fixated samples needs a long delipidation step (up to several months) [18,21]. On the other side, SWITCH/TDE protocol is still not optimized for paraffin-embedded samples [40] limiting its applicability on prolonged formalin-fixed brain samples. In the future, we plan to test the possibility of performing multi-round labelling of the tissue and carry out multiple antibody co-staining to implement the characterization of the specimens as already proposed by other authors [14,19,23].

To illustrate the versatility of the method, we used the SWITCH/TDE approach to prepare volumetric samples (10^{10} μm^3-sized volume) from different areas of the cerebral cortex from adult control subjects and pediatric patients with malformations of cortical development. The entire volumes, labeled with anti-NeuN antibody and DAPI, were acquired using a custom-made Two-Photon Fluorescence Microscope (TPFM) capable of performing mesoscopic reconstruction at sub-micron resolution. The optical sectioning and the high-resolution optical investigation made possible by TPFM, in combination with the tissue clearing technique, allowed imaging of the 3D organization of whole neurons lowering visual artifacts.

Volumetric imaging of samples generates a large amount of data (from tens of GB to tens of TB) that needs to be processed in an automated fashion to extract reliable and quantitative information. The software tools exploited in this study made it possible to analyze such big data. As a first step, we stitched together the 3D tiles acquired using the TPFM microscope. Adjacent tiles were aligned and merged by evaluating the cross-correlation of the overlapping areas using a custom-made software called Zetastitcher. Once stitched, we performed an automatic cell analysis using a 2.5D Machine Learning approach to perform neuronal mean volume assessment and cell counting. The volumetric assessment gives the possibility to extract morphological information that help to discriminate cell types using general staining as NeuN, reducing the labels necessary for the analysis (a critical point in human tissue preparation). We evaluated the accuracy of the 2.5D approach in different specimens but also along the stack depth to demonstrate that our analysis allows us to perform reliable quantitative evaluation of neuronal distributions in 3D showing that labeling with our clearing protocol is sufficient to provide enough contrast for the analysis.

Quantitative evaluations were performed on four different specimens (two different samples of prefrontal cortex from an adult and an elderly subject, one dysplastic brain sample from the left

Biomedical Optics EXPRESS

temporo-occipital cortex of a patient with FCDIIa, and one dysplastic brain sample from the left temporo-parietal cortex of a patient with HME) cleared with the SWITCH/TDE technique and acquired with the TPFM. The presented approach proved to be robust and applicable to the different specimens through the scanned surface and the depth. By mapping the neurons in 3D we characterized the cell density distribution and mean volume cells allowing us to assess the morphological differences between the arrangement of the layers in the analyzed samples. However, given the small number of samples we analyzed and the general purpose of this study, we did not assess the possible differences between control and dysplastic brain tissues.

Despite the innovation proposed here, there are still several points that need to be considered to obtain a faster, high-throughput, and informative automated characterization of tissue architecture. A combination with a faster optical technique, such as light-sheet microscopy, could facilitate scaling up the analysis. At the same time, further implementations of the automatic analysis methods could reduce the errors associated with neuronal counting and volume estimation. Nevertheless, we believe that our approach could be used in the future, not only to provide the anatomical description of samples but also to reduce interpretation biases and to obtain a more precise diagnostic neuropathological assessment. Indeed, morphological evaluation which still relies on traditional methods, cannot provide enough information for unequivocal classification. For example, MCD classification relies on an integrated diagnostic workflow which includes, in addition to histological evaluation, clinical, neuroradiological, and molecular investigations [9]. The 3D imaging approach we developed has the potential to introduce new classification paradigms that could solve conflicting situations. Identifying what is the minimum number of dysplastic neurons necessary to trigger seizures and how connections with the surrounding normal environment act on seizures spreading, is mandatory to better define the pathophysiology underlying FCD and related disorders. Traditional immunohistochemical methods based on the analysis of slices with $10 - 40$ μm of thickness do not allow an easy and univocal count of the number of abnormal cells in a given specimen or reconstruct all connections originating from and arriving at dysplastic cells. Although additional implementations are needed to selectively stain dysplastic cells, the goal of accurate cell and connection counting may be achieved through the analysis of large volumes of brain tissue, allowed by the protocol we describe. Indeed, the increase in statistical accuracy and the sensitivity of the assessment provided by 3D evaluations have already been demonstrated in tumors diagnosing and in stratifying patient prognosis [40].

Funding. Ministero della Salute (RF-2013-02355240); Horizon 2020 Framework Programme (785907, 945539); National Institute of Mental Health (1U01MH117023-01); Ministero dell'Istruzione, dell'Università e della Ricerca (Eurobioimaging Italian Nodes); Fondazione Cassa di Risparmio di Firenze.

Acknowledgments. We thank Raffaele Decaro from the University of Padova for providing a control human brain tissue specimen analyzed in this study. We express our gratitude to the donor involved in the body donation program of the Association des dons du corps du Centre Ouest, Tours, who made this study possible by generously donating his body to science. Bioretics srl, a company specialized in Machine Learning solutions for Computer Vision, is a subcontractor of LENS in the framework of the BRAIN Initiative Cell Census Network (n. 1U01MH117023-01). The content of this work is solely the responsibility of the authors and does not necessarily represent the official views of the National Institutes of Health. This research was supported by the EBRAINS research infrastructure, funded from the European Union's Horizon 2020 Framework Programme for Research and Innovation under the Specific Grant Agreement No. 945539 (Human Brain Project SGA3).

Disclosures. MR: Bioretics srl (I,E), GL, MN, and AS: Bioretics srl (E)

Data availability. Data underlying the results presented in this paper are available in Dataset 1, Ref. [38]. The raw data of the mesoscopic reconstructions and the ground truth masks are available on the EBRAINS platform Ref. [39]. Additional images other than the representative images are available from the corresponding author upon reasonable request.

Supplemental document. See Supplement 1 for supporting content.

References

1. A. Li, H. Gong, B. Zhang, Q. Wang, C. Yan, J. Wu, Q. Liu, S. Zeng, and Q. Luo, "Micro-optical sectioning tomography to obtain a high-resolution atlas of the mouse brain," Science **330**(6009), 1404–1408 (2010).

Biomedical Optics EXPRESS

2. T. Zheng, Z. Yang, A. Li, X. Lv, Z. Zhou, X. Wang, X. Qi, S. Li, Q. Luo, H. Gong, and S. Zeng, "Visualization of brain circuits using two-photon fluorescence micro-optical sectioning tomography," Opt. Express **21**(8), 9839–9850 (2013).
3. T. Jiang, B. Long, H. Gong, T. Xu, X. Li, Z. Duan, A. Li, L. Deng, Q. Zhong, X. Peng, and J. Yuan, "A platform for efficient identification of molecular phenotypes of brain-wide neural circuits," Sci. Rep. **7**(1), 13891 (2017).
4. T. Zheng, Z. Feng, X. Wang, T. Jiang, R. Jin, P. Zhao, T. Luo, H. Gong, Q. Luo, and J. Yuan, "Review of micro-optical sectioning tomography (most): technology and applications for whole-brain optical imaging," Biomed. Opt. Express **10**(8), 4075–4096 (2019).
5. T. Ragan, L. R. Kadiri, K. U. Venkataraju, K. Bahlmann, J. Sutin, J. Taranda, I. Arganda-Carreras, Y. Kim, H. S. Seung, and P. Osten, "Serial two-photon tomography for automated ex vivo mouse brain imaging," Nat. Methods **9**(3), 255–258 (2012).
6. K. Seiriki, A. Kasai, T. Hashimoto, W. Schulze, M. Niu, S. Yamaguchi, T. Nakazawa, K.-i. Inoue, S. Uezono, M. Takada, Y. Naka, H. Igarashi, M. Tanuma, J. A. Waschek, Y. Ago, K. F. Tanaka, A. Hayata-Takano, K. Nagayasu, and H. Hashimoto, "High-speed and scalable whole-brain imaging in rodents and primates," Neuron **94**(6), 1085–1100.e6 (2017).
7. J. Winnubst, E. Bas, T. A. Ferreira, Z. Wu, M. N. Economo, P. Edson, B. J. Arthur, C. Bruns, K. Rokicki, D. Schauder, D. J. Olbris, S. D. Murphy, D. G. Ackerman, C. Arshadi, P. Baldwin, R. Blake, A. Elsayed, M. Hasan, and J. Chandrashekar, "Reconstruction of 1, 000 projection neurons reveals new cell types and organization of long-range connectivity in the mouse brain," Cell **179**(1), 268–281.e13 (2019).
8. G. Clarke, S. Eidt, L. Sun, G. Mawdsley, J. Zubovits, and M. Yaffe, "Whole-specimen histopathology: a method to produce whole-mount breast serial sections for 3-D digital histopathology imaging," Histopathology **50**(2), 232–242 (2007).
9. I. Costantini, R. Cicchi, L. Silvestri, F. Vanzi, and F. S. Pavone, "In-vivo and ex-vivo optical clearing methods for biological tissues," Biomed. Opt. Express **10**(10), 5251–5267 (2019).
10. H.-U. Dodt, U. Leischner, A. Schierloh, N. Jährling, C. P. Mauch, K. Deininger, J. M. Deussing, M. Eder, W. Zieglgänsberger, and K. Becker, "Ultramicroscopy: three-dimensional visualization of neuronal networks in the whole mouse brain," Nat. Methods **4**(4), 331–336 (2007).
11. P. J. Keller and H.-U. Dodt, "Light sheet microscopy of living or cleared specimens," Curr. Opin. Neurobiol. **22**(1), 138–143 (2012).
12. H. R. Ueda, H.-U. Dodt, P. Osten, M. N. Economo, J. Chandrashekar, and P. J. Keller, "Whole-brain profiling of cells and circuits in mammals by tissue clearing and light-sheet microscopy," Neuron **106**(3), 369–387 (2020).
13. H. R. Ueda, A. Ertürk, K. Chung, V. Gradinaru, A. Chédotal, P. Tomancak, and P. J. Keller, "Tissue clearing and its applications in neuroscience," Nat. Rev. Neurosci. **21**(2), 61–79 (2020).
14. K. Chung, J. Wallace, S.-Y. Kim, S. Kalyanasundaram, A. S. Andalman, T. J. Davidson, J. J. Mirzabekov, K. A. Zalocusky, J. Mattis, A. K. Denisin, S. Pak, H. Bernstein, C. Ramakrishnan, L. Grosenick, V. Gradinaru, and K. Deisseroth, "Structural and molecular interrogation of intact biological systems," Nature **497**(7449), 332–337 (2013).
15. I. Costantini, J.-P. Ghobril, A. P. Di Giovanna, A. L. A. Mascaro, L. Silvestri, M. C. Müllenbroich, L. Onofri, V. Conti, F. Vanzi, L. Sacconi, R. Guerrini, H. Markram, G. Iannello, and F. S. Pavone, "A versatile clearing agent for multi-modal brain imaging," Sci. Rep. **5**(1), 9808 (2015).
16. M. Morawski, E. Kirilina, N. Scherf, C. Jäger, K. Reimann, R. Trampel, F. Gavriilidis, S. Geyer, B. Biedermann, T. Arendt, and N. Weiskopf, "Developing 3D microscopy with CLARITY on human brain tissue: Towards a tool for informing and validating MRI-based histology," NeuroImage **182**, 417–428 (2018).
17. K. Ando, Q. Laborde, A. Lazar, D. Godefroy, I. Youssef, M. Amar, A. Pooler, M.-C. Potier, B. Delatour, and C. Duyckaerts, "Inside alzheimer brain with clarity: senile plaques, neurofibrillary tangles and axons in 3-D," Acta Neuropathol. **128**(3), 457–459 (2014).
18. A. K. L. Liu, M. E. Hurry, O. T.-W. Ng, J. DeFelice, H. M. Lai, R. Pearce, G. T.-C. Wong, R. C.-C. Chang, and S. M. Gentleman, "Bringing clarity to the human brain: visualization of lewy pathology in three dimensions," Neuropathol. Appl. Neurobiol. **42**(6), 573–587 (2016).
19. E. Murray, J. H. Cho, D. Goodwin, T. Ku, J. Swaney, S.-Y. Kim, H. Choi, Y.-G. Park, J.-Y. Park, A. Hubbert, M. McCue, S. Vassallo, N. Bakh, M. P Frosch, V. J. Wedeen, H. S. Seung, and K. Chung, "Simple, scalable proteomic imaging for high-dimensional profiling of intact systems," Cell **163**(6), 1500–1514 (2015).
20. J. Phillips, A. Laude, R. Lightowlers, C. M. Morris, D. M. Turnbull, and N. Z. Lax, "Development of passive clarity and immunofluorescent labelling of multiple proteins in human cerebellum: understanding mechanisms of neurodegeneration in mitochondrial disease," Sci. Rep. **6**(1), 26013 (2016).
21. H. M. Lai, A. K. L. Liu, H. H. M. Ng, M. H. Goldfinger, T. W. Chau, J. DeFelice, B. S. Tilley, W. M. Wong, W. Wu, and S. M. Gentleman, "Next generation histology methods for three-dimensional imaging of fresh and archival human brain tissues," Nat. Commun. **9**(1), 2726 (2018).
22. Y.-G. Park, C. H. Sohn, R. Chen, M. McCue, D. H. Yun, G. T. Drummond, T. Ku, N. B. Evans, H. C. Oak, W. Trieu, H. Choi, X. Jin, V. Lilascharoen, J. Wang, M. C. Truttmann, H. W. Qi, H. L. Ploegh, T. R. Golub, S.-C. Chen, M. P. Frosch, H. J. Kulik, B. K. Lim, and K. Chung, "Protection of tissue physicochemical properties using polyfunctional crosslinkers," Nat. Biotechnol. **37**(1), 73–83 (2019).
23. T. Ku, W. Guan, N. B. Evans, C. H. Sohn, A. Albanese, J.-G. Kim, M. P. Frosch, and K. Chung, "Elasticizing tissues for reversible shape transformation and accelerated molecular labeling," Nat. Methods **17**(6), 609–613 (2020).

Biomedical Optics EXPRESS

24. T. Liebmann, N. Renier, K. Bettayeb, P. Greengard, M. Tessier-Lavigne, and M. Flajolet, "Three-dimensional study of alzheimer's disease hallmarks using the idisco clearing method," Cell Rep. **16**(4), 1138–1152 (2016).
25. F. Casoni, S. A. Malone, M. Belle, F. Luzzati, F. Collier, C. Allet, E. Hrabovszky, S. Rasika, V. Prevot, A. Chédotal, and P. Giacobini, "Development of the neurons controlling fertility in humans: new insights from 3D imaging and transparent fetal brains," Development **143**(21), 3969–3981 (2016).
26. S. Hildebrand, A. Schueth, A. Herrler, R. Galuske, and A. Roebroeck, "Scalable labeling for cytoarchitectonic characterization of large optically cleared human neocortex samples," Sci. Rep. **9**(1), 10880–10 (2019).
27. S. Zhao, M. I. Todorov, R. Cai, A.-M. Rami, H. Steinke, E. Kemter, H. Mai, Z. Rong, M. Warmer, K. Stanic, O. Schoppe, J. C. Paetzold, B. Gesierich, M. N Wong, T. B. Huber, M. Duering, O. T. Bruns, B. Menze, J. Lipfert, V. G. Puelles, E. Wolf, I. Bechmann, and A. Ertürk, "Cellular and molecular probing of intact human organs," Cell **180**(4), 796–812.e19 (2020).
28. G. Mazzamuto, "ZetaStitcher: a tool for large volumetric image stitching," GitHub, https://github.com/lens-biophotonics/ZetaStitcher/.
29. I. Constantini, G. Mazzamuto, M. Roffilli, A. Laurino, F. Castelli, M. Neri, G. Lughi, A. Simonetto, E. Lazzeri, L. Pesce, C. Destrieux, L. Silvestri, V. Conti, R. Guerrini, and F. Pavone, "3D reconstruction and analysis of four human brain cortex samples with two-photon fluorescence microscopy [Data set]," EBRAINS (2020) https://doi.org/10.25493/SNWB-YQR.
30. G. Mazzamuto, I. Costantini, M. Neri, M. Roffilli, L. Silvestri, and F. S. Pavone, "Automatic segmentation of neurons in 3D samples of human brain cortex," in *International Conference on the Applications of Evolutionary Computation*, (Springer, 2018), pp. 78–85.
31. M. Lin, Q. Chen, and S. Yan, "Network in network," arXiv preprint (2013).
32. W. E. Lorensen and H. E. Cline, "Marching cubes: A high resolution 3D surface construction algorithm," SIGGRAPH Comput. Graph. **21**(4), 163–169 (1987).
33. Bioretics srl, "ALIQUIS," Available at https://www.bioretics.com/aliquis.
34. M. Abadi, A. Agarwal, P. Barham, E. Brevdo, Z. Chen, C. Citro, G. S. Corrado, A. Davis, J. Dean, M. Devin, S. Ghemawat, I. Goodfellow, A. Harp, G. Irving, M. Isard, Y. Jia, R. Jozefowicz, L. Kaiser, M. Kudlur, J. Levenberg, D. Mané, R. Monga, S. Moore, D. Murray, C. Olah, M. Schuster, J. Shlens, B. Steiner, I. Sutskever, K. Talwar, P. Tucker, V. Vanhoucke, V. Vasudevan, F. Viégas, O. Vinyals, P. Warden, M. Wattenberg, M. Wicke, Y. Yu, and X. Zheng, "TensorFlow: Large-scale machine learning on heterogeneous systems," (2015). Software available from tensorflow.org.
35. Bioretics srl, "LAIRA,", Available at https://laira.bioretics.com.
36. B. Settles, "Active learning literature survey," Tech. rep., University of Wisconsin-Madison Department of Computer Sciences (2009).
37. Bioretics srl, "Ximage," GitHub, https://github.com/bioretics/ximage.
38. I. Constantini, G. Mazzamuto, M. Roffilli, A. Laurino, F. Castelli, M. Neri, G. Lughi, A. Simonetto, E. Lazzeri, L. Pesce, C. Destrieux, L. Silvestri, V. Conti, R. Guerrini, and F. Pavone, "Assessment of the 2.5D segmentation," figshare, (2021) https://doi.org/10.6084/m9.figshare.13273184.
39. S. Lucasfilm Ltd, "Alembic," http://www.alembic.io.
40. N. Tanaka, S. Kanatani, R. Tomer, C. Sahlgren, P. Kronqvist, D. Kaczynska, L. Louhivuori, L. Kis, C. Lindh, and P. Mitura, "Whole-tissue biopsy phenotyping of three-dimensional tumours reveals patterns of cancer heterogeneity," Nat. Biomed. Eng. **1**(10), 796–806 (2017).